Chem Biol Drug Des 2013; **82:** 296–306

Research Article

Chitosan-Coated Superparamagnetic Iron Oxide Nanoparticles for Doxorubicin Delivery: Synthesis and Anticancer Effect Against Human Ovarian Cancer Cells

Amaneh Javid[1], Shahin Ahmadian[1,2,*], Ali A. Saboury[1], Seyed M. Kalantar[3] and Saeed Rezaei-Zarchi[4]

[1]Department of Biochemistry, Institute of Biochemistry and Biophysics, University of Tehran, Tehran, Iran
[2]Center of Excellence of Nano-Biomedicine, Nano-Science and Nano-Technology Research Center, University of Tehran, Tehran, Iran
[3]Research and Clinical Centre for Infertility, Shahid Sadoughi University of Medical Sciences, Yazd, Iran
[4]Department of Biology, Payame Noor University, Yazd, Iran
**Corresponding author: Shahin Ahmadian, ahmadian@ibb.ut.ac.ir*

Doxorubicin-loaded chitosan-coated superparamagnetic iron oxide nanoparticles (Fe_3O_4; SPIO-NPs) were prepared by coprecipitation and emulsification cross-linking method and uniform NPs with an average particle size of 82 nm, with high encapsulation efficiencies, were obtained. The drug-loading efficiency of doxorubicin (3.2 mg/mg NPs) showed better results for the chitosan-loaded SPIO-NPs as compared to the bare ones (0.5 mg/mg; $p < 0.05$). The incubation of A2780 and OVCAR-3 human ovarian cancer cells with doxorubicin-loaded and doxorubicin-loaded chitosan-coated SPIO-NPs, for 24, 48, 72, 96, and 120 h, showed significant IC_{50} (2.0 ± 0.6 and 7.1 ± 2.7 mM doxorubicin) and IC_{90} (4.0 ± 9.2 and 10 ± 0.5 mM doxorubicin), respectively, after 96 h of incubation. While, 95% and 98% growth inhibition was seen in A2780 and OVCAR-3 cells after the 96-h exposure to the doxorubicin-chitosan-SPIO-NPs ($p < 0.05$). A 5-day (120 h) incubation with doxorubicin-chitosan-SPIO-NPs showed that A2780 and OVCAR-3 cells were able to uptake 120 and 110 pg iron/cell, respectively, when treated with doxorubicin-chitosan-SPIO-NPs for 72 h ($p < 0.05$).

Key words: chitosan, doxorubicin, drug loading, encapsulation, human ovarian cancer, iron oxide

Received 19 October 2012, revised 8 March 2013 and accepted for publication 2 April 2013

Nanotechnology is at the leading edge of the rapidly developing new therapeutic and diagnostic concepts in all areas of medicine (1). The magnetite nanoparticles with a small size, narrow particle size distribution and high magnetization values had been used widely in targeted drug delivery (2), for the treatment of different cancers (3). Because nanoparticles are a 100–1000 times smaller than a human cell, nanoscale devices can enter cells and the organelles easily and interact with DNA, proteins, enzymes, and cell receptors extracellularly and intracellularly. Because the biological processes, including the events that lead to cancer, occur at the nanoscale level and inside the cells, nanotechnology offers tools that may be able to detect disease in a very small volume of cells or tissue. In general, nanotechnology may offer a faster and more efficient means for scientists to do much of what they do now (4).

The ability of SPIO-NPs to be functionalized and concurrently respond to a magnetic field has made them a useful tool for theranostics – the fusion of therapeutic and diagnostic technologies that targets to individualize medicine (5). Fe_3O_4 are superior to other metal oxide nanoparticles for their biocompatibility and stability and are, by far, the most commonly employed SPIO-NPs for biomedical applications. Recently, considerable research has been focused on iron oxides due to their potential uses such as magnetic drug targeting, magnetic resonance imaging for clinical diagnosis, recording material and catalysts (6). Surface modification can stabilize magnetite nanoparticles in the physiological environment and functionalize them to make them responsive to the physical stimuli (7).

Iron oxide nanoparticles can be engineered with desired functionality. The techniques used for surface functionalization comprise grafting of or coating with organic species, including surfactants or polymers (8,9). The biocompatible surface coating not only stabilizes the iron oxide nanoparticles, but also provides accessible surface for the biomolecular conjugation through the well-developed bioconjugation chemistry for biomedical applications (10,11). In addition, multiple grafting or coating of small molecules can provide multivalent systems that exhibit significantly enhanced efficacy towards the drugs and biomolecules (12). Degradable polymeric nanoparticles are the most optimal choice for use as anticancer agents due to their unusual beneficial properties, most notably enhanced drug availability for prolonging the drug effects in tumor tissues (13). However, with respect to free

 doi: 10.1111/cbdd.12145

drugs, these drug loaded nanoparticles have been shown to decrease the permeability of the drugs across the cell membrane (14).

Chitosan, a natural compound and a deacetylated derivative of chitin, is a positively charged polymer carrier. The cell adhesion and potential uptake of chitosan particles are also most favorable due to their attraction to negatively charged cell membranes, an attractive feature for the treatment of solid tumors (15,16). Moreover, chitosan has shown favorable biocompatibility (17) as well as the ability to increase cell membrane permeability both *in vitro* (18) and *in vivo* (19). Among the various biopolymers, chitosan along with nanoparticles has been utilized as a stabilizing agent due to its excellent film-forming ability, mechanical strength, biocompatibility, non-toxicity, high permeability towards water, susceptibility to chemical modifications, cost-effectiveness (20).

Keeping in mind the novel properties of the magnetic nanoparticles, the Fe_3O_4 nanoparticles were modified with chitosan and loaded with the anticancer drug doxorubicin (DOX) for achieving a biocompatible, biodegradable and site-specific carrier of anticancer drugs. The effect of these drug loaded nanocomposits was also evaluated on biochemical and morphological parameters of the human ovarian cancer cell lines of A2780 and OVCAR-3.

Experimental Section

Chemicals

Doxorubicin and chitosan (low molecular weight; viscosity, 20 cps) were purchased from Sigma-Aldrich Chemical Co. (St. Louis, MO, USA). RPMI-1640 medium and all of the additives were purchased from GIBCO Co. (Grand Island, NY, USA). The ovarian cancer cell lines, A2780 (NCBI code, C461) and OVCAR-3 (NCBI code, C430) were purchased from Pasteur Institute, Tehran, Iran. All other chemicals, used, were of the highest purity and biological grade available from the commercial sources.

Synthesis of chitosan-coated iron oxide NPs

Chitosan-coated iron oxide (Fe_3O_4) NPs were prepared by coprecipitation technique, with some modifications in the previously reported method (21,22). Firstly, 5.41 g of $FeCl_3{\cdot}6H_2O$ (99% purity) and 1.99 g $FeCl_2{\cdot}4H_2O$ (99% purity) were dissolved in 100 mL of distilled water in a three-necked flask. The reaction principle is as follows:

$$Fe^{2+} + 2Fe^{3+} + 8OH^- \leftrightarrow Fe(OH)_2 + 2Fe(OH)_3 \rightarrow Fe_3O_4 + 4H_2O$$

Chitosan molecules were coated onto the surface of SPIO-NPs, by adsorbing them onto SPIO-NPs, simultaneously during their synthesis. As the chitosan is not water soluble, a 1% (w/v) aqueous solution was made by adding 0.2 g of chitosan into a mixture of water (19 mL) and a 2 N acetic acid (1 mL). The pH of the mixture (100 mL) of aqueous solutions (0.5 M) of iron chloride ($FeCl_2$ + $FeCl_3$) and diluted chitosan (0.05% (w/v) was maintained at pH 6.9 through the slow addition of 25 mL of the aqueous NH_4OH (25–28%, w/w) while stirring constantly under the protection of dry nitrogen at 80 °C (23). Pressurized air was supplied to the above solution to oxidize Fe^{2+} to Fe^{3+} for the formation of magnetite (Fe_3O_4) (24–26). Change in the color of solution to dark brown to black, due to the precipitation of Fe_3O_4, indicates the formation of bare or chitosan-coated SPIO-NPs (21,22). The tetramethyl ammonium hydroxide was used as the surfactant, in preparing the bare SPIO-NPs, to maintain the aqueous solution of bare SPIO-NPs in the state of colloidal suspension. The supernatant was discarded and the resulting precipitate was collected with strong magnet and rinsed thrice with distilled water to remove excess NH_4OH.

Characterization of synthesized NPs

FT-IR analysis of bare Fe_3O_4 (SPIO-NPs), chitosan and SPIO-NPs + chitosan was carried out, via FT-IR Spectrophotometer (Model 8300; Shimadzu Corporation, Tokyo, Japan), to investigate the presence of chitosan coating on the surface of SPIO-NPs. Transmission electron microscope (TEM) and IR results are important because they evidenced the successful coating of SPIO-NPs by chitosan. Size and surface morphology of the synthesized NPs were characterized with the help of TEM (H-7600; Hitachi High-Technologies Corporation, Tokyo, Japan). A dynamic light scattering spectrometer (DLS-7000AL; Otsuka Electronics, Osaka, Japan) was used to determine the average diameters of the bare and the coated NPs.

Conjugation of DOX to the chitosan-coated SPIO-NPs

For drug conjugation to modified SPIO-NPs, different concentrations (0, 10, 30, 50, 70, 100, 150, and 200 μg) of chitosan-coated SPIO-NPs were first sonicated with 0.1, 0.2, 0.3, 0.4, 0.5, 1.0, 1.5, 2.0, 2.5, and 3.0 mg/mL concentrations of DOX solution for 0.5 h and then stirred overnight at room temperature in the dark. All the samples were centrifuged at 18 000 × g for 1 h. The DOX concentration of all the samples was measured using a standard DOX concentration curve, generated with a UV-Vis spectrophotometer at the wavelength of 233 nm. The drug conjugation to the chitosan modified SPIO-NPs has been illustrated in Figure 1.

Loading efficiency of incorporated drug

The quantification and release kinetics of the drug-loading onto the modified SPIO-NPs was carried out through UV/Visible double-beam spectrophotometer (Hitachi U-2000) at 200–800 nm. Drug incorporation efficiency was observed

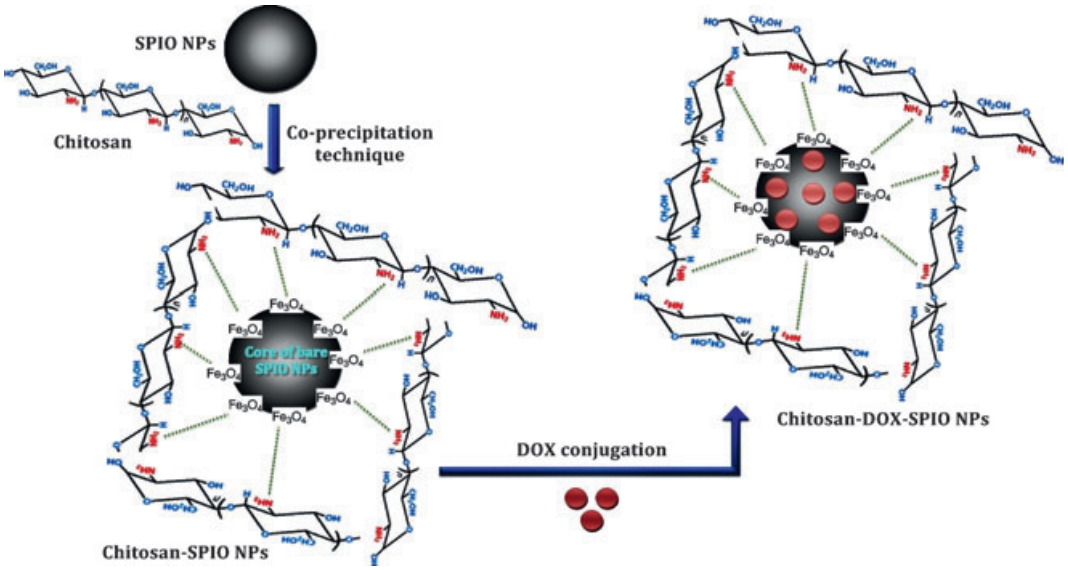

Figure 1: Illustration of the modification mechanism of SPIO-NPs with chitosan, followed by doxorubicin (DOX) loading.

both as drug loading (% w/w) and drug entrapment (%), by the below-stated eqns (1) and (2), respectively.

$$\text{Drug loading}\,(\%\text{w/w}) = \frac{\text{Mass of drug loaded in NPs} \times 100}{\text{Mass of nanoparticles}} \quad (1)$$

$$\text{Drug entrapment}\,(\%) = \frac{\text{Mass of drug loaded in NPs} \times 100}{\text{Mass of drug used in formulation}} \quad (2)$$

Cancer cell culture

The human ovarian cancer cell lines, A2780 and OVCAR-3, were maintained in RPMI-1640 medium, supplemented with 10% (v/v) FBS, 0.25 IU/mL insulin, 100 μg/mL streptomycin, 100 units/mL penicillin and 0.3 mg/mL glutamine. Cells were cultured at 37 °C in a humidified atmosphere of 5% (v/v) CO_2 in air. For cytotoxicity data, clonogenic assay was used. Clonogenic assay is used for studying the effectiveness of specific agents on the survival and proliferation of cells. For this assay, 500 cells from each cell line were plated into 60-mm tissue culture dishes 24 h prior to nanomedicine treatment. Cells were then treated, in triplicate, with 50 μg/mL of the: (i) SPIONs alone, (ii) chitosan-coated SPIO-NPs, and (iii) DOX-chitosan-SPIONs for 4 h, after which the experimental media were removed and fresh medium was added to the cells. Incubation was continued until the colonies of approximately 50 cells were observed (7–9 days). Growth medium was replaced with fresh medium on day 5. The resulting colonies were stained with 1 mL of the clonogenic reagent for 45 min, washed with PBS, blue colonies were counted and the data were compared with those of the control according to the following relation:

$$\text{Percent survival} = (\text{Average treated count/Average control count}) \times 100$$

Analysis of iron uptake by cancer cells

To quantitate the iron uptake by cancer cell lines, the A2780 and OVCAR-3 cells were grown (~10^5 cells/1 mL medium) with and without 0.5 mg/mL of bare, chitosan-coated, and chitosan-coated and drug-loaded SPIO-NPs in 24-well culture plates. Cells were washed with PBS, resuspended, counted, centrifuged down, and the cell pellets were dissolved in 37% HCl solution at 70–80 °C for 30 min. The samples were diluted to a final iron concentration of 1.0–5.0 μg/mL. Three replicates of each sample were measured using an inductively coupled plasma emission spectroscopy (ICP ES) and the results were averaged with standard deviation.

Cell viability and apoptosis analyses

Viability was determined by staining cancer cells with 1% methylene blue in 70% ethanol, followed by three washes in de-ionized water. Data obtained were used to calculate the IC_{50} and IC_{90} values for each cell line, administered with DOX-chitosan-SPIO-NPs. For all experiments, 3 × 10^6 cells from each cell line were plated into 150 mm tissue culture dishes, 24 h prior to the nano-composite treatment. In order to determine the corresponding IC_{50} and IC_{90} values, the cells were separately treated with the as-prepared bare, coated and drug-loaded nano-composites for 24, 48, 72, 96, and 120 h at 37 °C. Plates were washed thrice with PBS and incubated in 10 mL of fresh medium for an additional 48 h before the final cell collection. All the cells were collected by sedimenting at 2000 × *g* for 5 min.

For the 5-dimethylthiazol-2-yl-2,5-diphenyltetrazolium bromide (MTT) assay, A2780 and OVCAR-3 cells were plated in 96-well plates and exposed to uncoated SPIO-NPs, chitosan-SPIO-NPs and DOX-chitosan-SPIO-NPs at a concentration of 50 μg/mL for 24, 48, 72, 96, and 120 h. After the culture period, the medium was removed from each well and replaced with fresh medium. Cellular apoptosis was detected by Annexin-V-FLUOS staining and studied with the help of flow cytometry.

Immuno-blot analysis and investigation of gene expression

A2780 and OVCAR-3 cells were lysed in a buffer containing 50 mM Tris/HCl (pH 7.4), 150 mM NaCl, 1 mM EDTA, 0.2% (v/v) Nonidet P40, and protease inhibitor cocktail in ice for a period of 10 min. Cell debris was pelleted by centrifugation, and the total protein concentration of the soluble extracts was determined by Bradford assay, according to the manufacturer's instructions. Total soluble protein extract (30 μg) for each sample was resolved by SDS PAGE (12% gels). After electrophoresis, the survivin, Bcl-2, Bax and NF-κB proteins were transferred to nitrocellulose, and the blot was blocked for 1 h at room temperature with a solution of 5% dried milk in PBST (0.1% (v/v) Tween 20 in PBS). The blot was incubated, overnight at 4 °C, with either of the anti-Bcl-2 monoclonal antibody, anti-Bax, anti-NF-κB and anti–survivin polyclonal antibodies to evaluate the levels of protein expression. Primary antibodies were detected using an horseradish peroxidase conjugated secondary antibody and enhanced chemiluminescence was taken as described by the manufacturer.

Statistical analyses

Results are presented as mean ± standard deviation. The two-way ANOVA and the Student's *t*-test were used to compare data from the different treatment groups. Statistical significance was accepted at $p < 0.05$.

Results and Discussion

Synthesis of bare and chitosan-coated SPIO-NPs

The bare and chitosan-coated SPIO-NPs were synthesized by coprecipitation technique. As the chitosan can precipitate under alkaline conditions, when 2 mL NaOH (1.0 M) was added to the acidic solution containing the chitosan, Fe(II) and Fe(III) ions, the SPIO-NPs were formed during the precipitation of chitosan, leading to the formation of chitosan-coated SPIO-NPs.

Characterization of bare and chitosan coated SPIO-NPs

FT-IR analysis

The bonding status of chitosan molecules on the surface of the particle could be checked from the wavelength-dependent data of transmittance obtained using an FTIR spectrometer. According to the the SPIO-NPs spectrum of Figure 2, the 576.25/cm region of the Fe_3O_4 spectrum represents the Fe-O group while, the 3401.82/cm peak in the chitosan spectrum is related to the primary amine group. The stretching vibrations of O-H and C-H can be seen through the peaks of 2919 and 2874/cm. While in the SPIO-NPs + chitosan spectrum, the bio-sorption peak of primary amine (–NH_2) is demonstrated by 3392.17 and 1613.56/cm. The bio-sorption bands around 1078.01/cm show the stretch vibration of C–O bond and the 584.32/cm band represents the Fe-O group of SPIO-NPs. So, the FT-IR analysis supports the notion that the chitosan coating is present onto the surface of SPIO-NPs.

Microscopic analysis

The synthesized bare and chitosan coated NPs were characterized by atomic force microscope and the final diameters were obtained to be 10 and 69.0 nm (Figure 3A, B). The size of prepared nanoparticles was also determined by TEM analysis. Figure 3C shows the TEM (H-7600; Hitachi) micrographs of bare nanoparticles, while Figure 3D demonstrates the TEM micrograph of chitosan-coated SPIONs.

Dynamic light scattering analysis

Size distribution of the synthesized SPIO-NPs and chitosan-coated SPio-NPs was investigated in an aqueous solution with the help of dynamic light scattering (DLS) spectrometer. As shown in Figure 4A, B), the mean diameter of the chitosan-SPIO-NPs was recorded to be about 69.0 nm. The size distribution of the bare SPIO-NPs was also determined and recorded to be about 10 nm.

Doxorubicin loading onto the chitosan-coated SPIO-NPs

To assess the conjugation capacity of DOX the modified NPs, the following concentrations of the drug: 0.1, 0.2, 0.3, 0.4, 0.5, 1.0, 1.5, 2.0, 2.5, and 3.0 mg/mL were added to the chitosan-modified NPs and incubated for 30 min and then stirred overnight at room temperature in the dark. A DOX concentration curve (233 nm) was constructed from standard solutions. As shown in Figure 5A, DOX loading of modified SPIO-NPs at an initial drug concentration of 0.5 mg/mL was nearly saturating.

IC_{50} and IC_{90} analyses of the A2780 and OVCAR-3 cell lines, after 24, 48, 72, 96, and 120 h (5 days) exposure to DOX-loaded chitosan-coated SPIO-NPs, were recorded at 2.0 ± 0.6 and 7.1 ± 2.7 mM concentration of drug, while, IC_{90} of both cell lines was seen at 4.0 ± 9.2 and 10 ± 0.5 mM DOX concentration after 96 h. This demonstrates that the OVCAR-3 cells were more resistant to the lower concentrations of drug as compared to the A2780 cells (Table 1; $p < 0.05$).

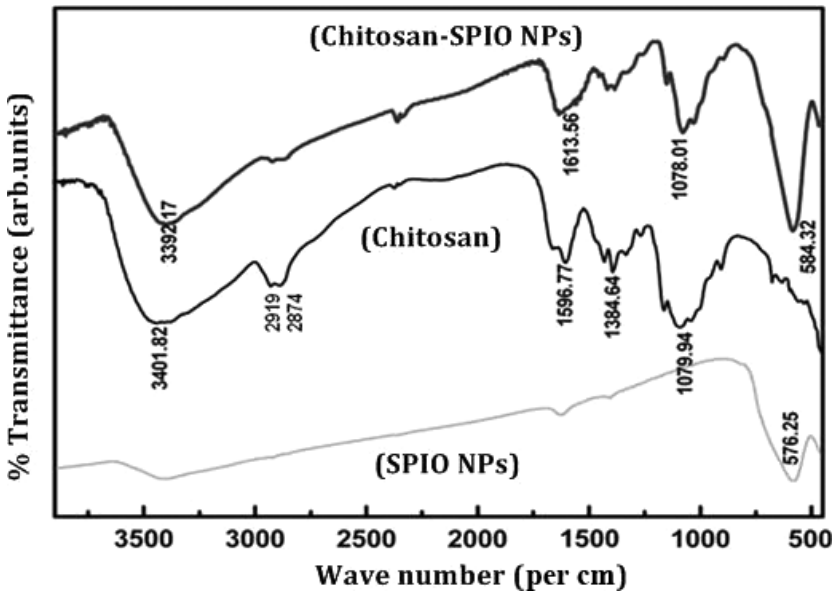

Figure 2: FT-IR spectra of bare SPIO-NPs, chitosan, and SPIO-NPs + chitosan.

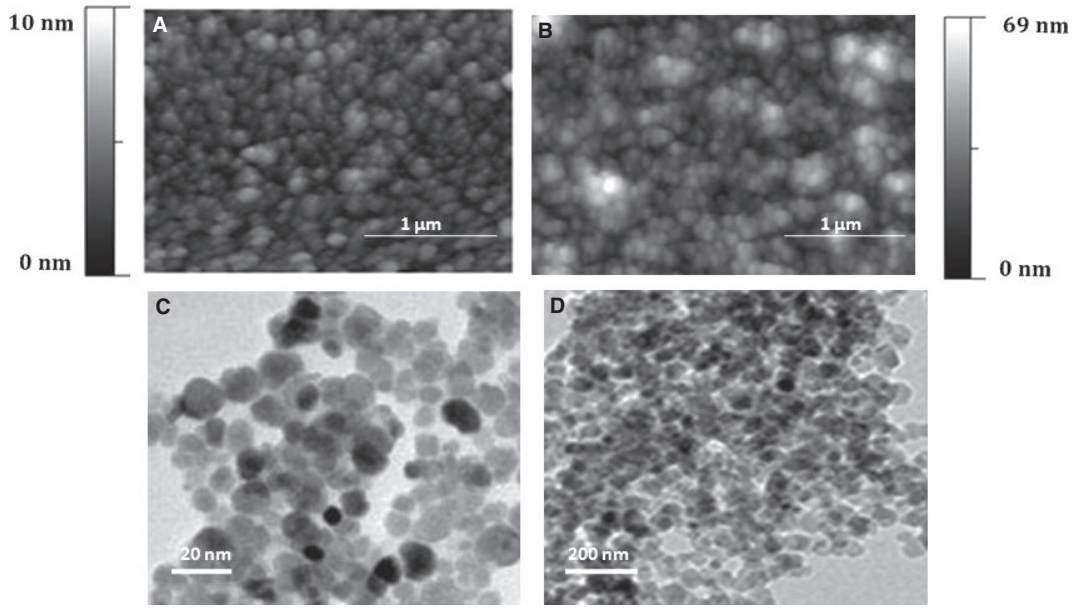

Figure 3: (A, C) Atomic force and transmission electron microscopic images of the bare SPIO-NPs, B, D) atomic force microscope (AFM) and transmission electron microscope (TEM) images of chitosan-modified SPIONs, respectively.

DOX release profile

Figure 5B shows the DOX release profiles of the free and the conjugated drug, at the pH range of 1.5–7.0. At pH 7.0, a small amount of the drug release was observed after the incubation period of 48 h. This is a desirable characteristic as the pH 7.4 is the undesired pH for the proper release of the drugs from the nanoconjugated drug carrier. This will also prevent the premature release of the drugs before the nanoconjugates reach the cancer cells. Figure 5B shows that the pH 6.0 provided the desirable conditions for the proper drug release. The first 10 h represent the period of initial rapid release, followed by a steady state. This pH-dependent drug release behavior is favorable for the chemotherapeutic process as it can significantly reduce the preterm drug release on the body pH level (pH 7.4) and maximizing the amount of drug reaching the target tumor cells, once the drug-loaded SPIO-NPs internalize and enter the tumor by endocytosis (pH 4.5–6.5).

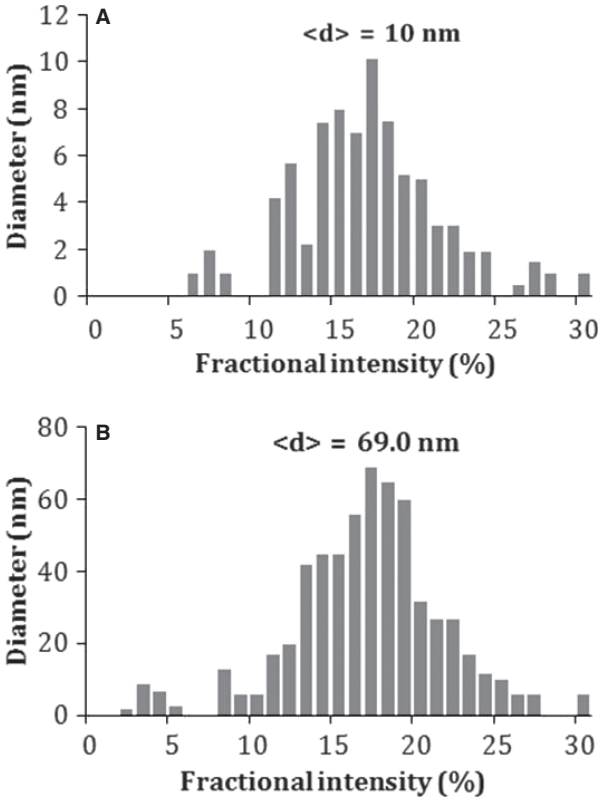

Figure 4: Demonstration of size distribution of (A) bare SPIO-NPs and (B) chitosan-SPIO-NPs in an aqueous solution with the help of dynamic light scattering (DLS) spectrometer. The mean diameter of the chitosan-SPIO-NPs was recorded to be about 69.0 nm. The size distribution of the bare ferrite particles is also shown here. The mean diameter of the bare particles was about 10 nm.

Cell culture and iron uptake by cancer cells

The human ovarian cancer cell lines were cultured in RPMI-1640 culture medium for a period of 120 h (5 days). The nanoparticle uptake by the human ovarian cancer cell lines of A2780 and OVCAR-3 was evaluated after the cells were grown in medium containing 0.2 mg/mL NPs for up to 5 days. Figure 6 shows the uptake of bare, DOX-loaded and DOX-loaded chitosan-coated SPIO-NPs by A2780 and OVCAR-3 ovarian cancer cell lines. The bare SPIO-NPs were internalized into the cells quickly (14 pg iron/cell) within the first day, while the uptake amount showed fluctuations during the following 4 days, probably due to the fast growth of cancer cells. The uptake of 3 pg iron/cell was recorded after a culture period of 5 days. After the chitosan coating and drug loading, the nanoparticle uptake by cancer cells increased significantly with the passage of time. An iron uptake of 97 and 90 pg/cell was seen in A2780 and OVCAR-3 cells, respectively, after an incubation period of 3 days. The average uptake of drug loaded chitosan-coated NPs by A2780 and OVCAR-3 cells during the 5 days was 89 and 100 pg/cell. This might be attributed to the fact that the presence of polymer prevents the nanoparticle agglomeration in the culture medium and makes it more soluble and an easy-to-pass entity through the cell membrane.

Table 2 shows the results of growth inhibition analysis. Our results state that the administration of DOX-loaded (0.5 mg/mL) and chitosan-coated SPIO-NPs caused 98% and 95% growth inhibition in A2780 and OVCAR-3 cell lines, during a culture period of 96 h, respectively. These results were compared with those of the effect of 0.5 mg/mL free DOX (80% and 82% for A2780 and OVCAR-3 cells) and the DOX-loaded SPIO-NPs (83% and 84% for A2780 and OVCAR-3 cells) under same experimental conditions ($p < 0.05$).

Cytotoxicity and synergistic effect of DOX-chitosan-SPIO-NPs on the cancer cells

For the cytotoxicity analysis, A2780 and OVCAR-3 cells were treated separately with DOX, SPIO-NPs, chitosan-SPIO-NPs and DOX-chitosan-SPIO-NPs for 24 h. Apoptotic cell death was analyzed by staining the cells with Annexin-V-FLUOS staining kit and analyzed by flow cytometry. The results revealed a dose-dependent induction of early or late apoptotic cell death in these two cell lines (Figure 7). Compared to OVCAR-3 cells, the A2780 cells showed more cell death. A2780 cells showed 91% apoptosis after the administration of DOX-loaded chitosan-SPIO-NPs (5 mg/L; $p < 0.05$). While, 87.1% apoptosis was seen in the OVCAR-3 cells under same conditions ($p < 0.05$), which indicates that chitosan-modified SPIO-NPs could enhance the DOX-induced apoptosis in both of the human ovarian cancer cell lines.

Western blot analysis for gene expression

In the Western blot analysis, the survivin and bcl-2 were used as the representatives of the inhibitor of apoptosis protein. During the present study, the expression of bax, bcl-2, NF-κB and survivin proteins was also studied in the A2780 and OVCAR-3 cells, treated with DOX alone, bare SPIO-NPs, chitosan-coated SPIO-NPs and DOX- chitosan-SPIO-NPs, respectively. According to Figure 8, the results have shown that the level of bcl-2 and survivin proteins had a sharp decrease while NF-κB was also regulated in the cultures, treated with DOX-chitosan-SPIO-NPs in A2780 and OVCAR-3 cells (Figure 8A, B). This represents the activation of apoptotic mechanism in cancer cells after the nanoparticle-based DOX delivery *in vitro* ($p < 0.05$).

The SPIO-NPs have a proven candidacy for their biocompatibility and wide applications in the medical field (24). During the present study, the bare and chitosan coated superparamagnetic iron oxide (SPIO) nanoparticles were synthesized by the coprecipitation technique. The synthesized chitosan-coated nanoparticles had the diameter of about 69 nm, which was confirmed by both of

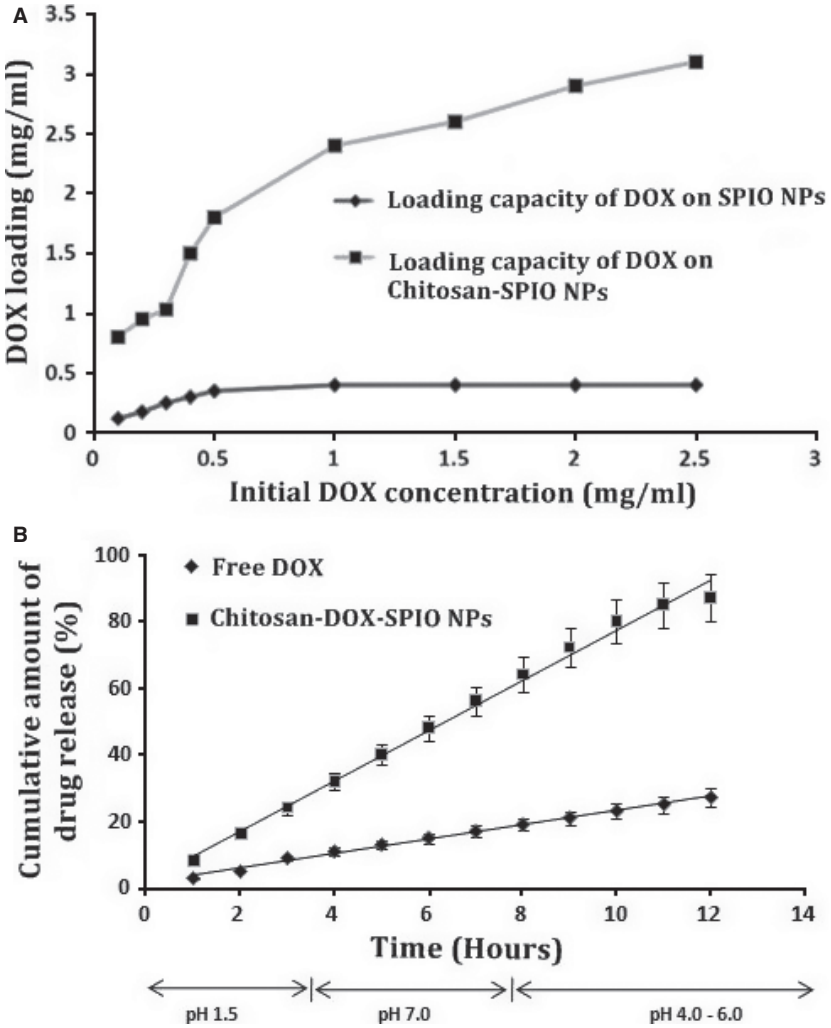

Figure 5: (A) Doxorubicin loading onto the chitosan-coated SPIO-NPs. Doxorubucin concentrations of 0.1, 0.2, 0.3, 0.4, 0.5, 1.0, 1.5, 2.0, 2.5, and 3.0 mg/mL were added to the chitosan-modified SPIO-NPs and incubated for 30 min and then stirred overnight at room temperature in the dark and the measurements were carried out with the help of UV-Visible spectrophotometer at the wavelength of 233. (B) *In vitro* release profile of doxorubicin (DOX) from chitosan-coated SPIO-NPs at different pH values at 37 °C, after the incubation period of 48 h (n = 3).

the TEM and DLS techniques that shows that no aggregation of the nanoparticles occurred in solution. Numerous polymer-based nanoparticles have been developed for cancer-targeted delivery of therapeutic agents (25).

The polysaccharide coating may provide steric protection against protein adsorption and macrophage uptake. Additionally, as polysaccharides offer many available reactive groups, active targeting could be obtained by grafting ligands onto the nanoparticle surface (Figure 1). Because chitosan has high affinity for cell membranes due to its mucoadhesive properties and positive charge, it was utilized as a coating agent for magnetic nanoparticles, during the present study. The presence of a chitosan coating was also studied using zeta potential measurements. Indeed, chitosan-coated nanoparticles had positive (+38 mV) zeta potential value (26).

Drug loading is affected by particle size. Preparations of smaller particles have larger total surface area. Therefore, most of the drug associated would be at or near the particle surface, leading to fast drug release. Whereas, larger particles have large cores, which allow more drug to be encapsulated and slowly diffuse out (27). Our results have shown that the DOX-loaded and chitosan-coated SPIO-NPs showed better drug delivery and release performance as compared to the bare nanoparticles.

Apoptosis can be prompted in the cancer cells either by activating the proteins upstream of apoptotic signaling pathway or by inhibiting the antiapoptotic factors. An overexpression of survivin is seen in all the human cancers. The presence or the overly expressed survivin means resistance to apoptosis, which is associated with increased malignancy

Table 1: IC_{50} and IC_{90} of A2780 and OVCAR-3 cell lines after 24, 48, 72, 96, and 120 h (5 days) exposure to DOX-loaded chitosan-coated SPIO-NPs

	24 h	48 h	72 h	96 h	120 h
Type of cell line	IC_{50} for DOX-loaded chitosan-modified SPIO-NPs (mM)				
A2780	3.6 ± 4.5	2.7 ± 0.9	2.3 ± 4.5	2.0 ± 0.6	2.0 ± 0.6
OVCAR-3	14 ± 1.5	11 ± 0.9	8.6 ± 0.5	7.1 ± 2.7	7.11 ± 0.8
	IC_{90} for DOX-loaded chitosan-modified SPIO-NPs (mM)				
A2780	8.5 ± 0.2	7.2 ± 0.9	6.5 ± 0.8	4.0 ± 9.2	3.8 ± 1.0
OVCAR-3	19 ± 4.5	17.2 ± 3.7	14.9 ± 1.7	10 ± 0.5	8.8 ± 3.7

DOX, doxorubicin. The IC_{50} and IC_{90} are defined as the concentrations causing 50% and 90% growth inhibition in treated cells, respectively, when compared to control cells. Values are means ± SEM of at least three separate experiments.

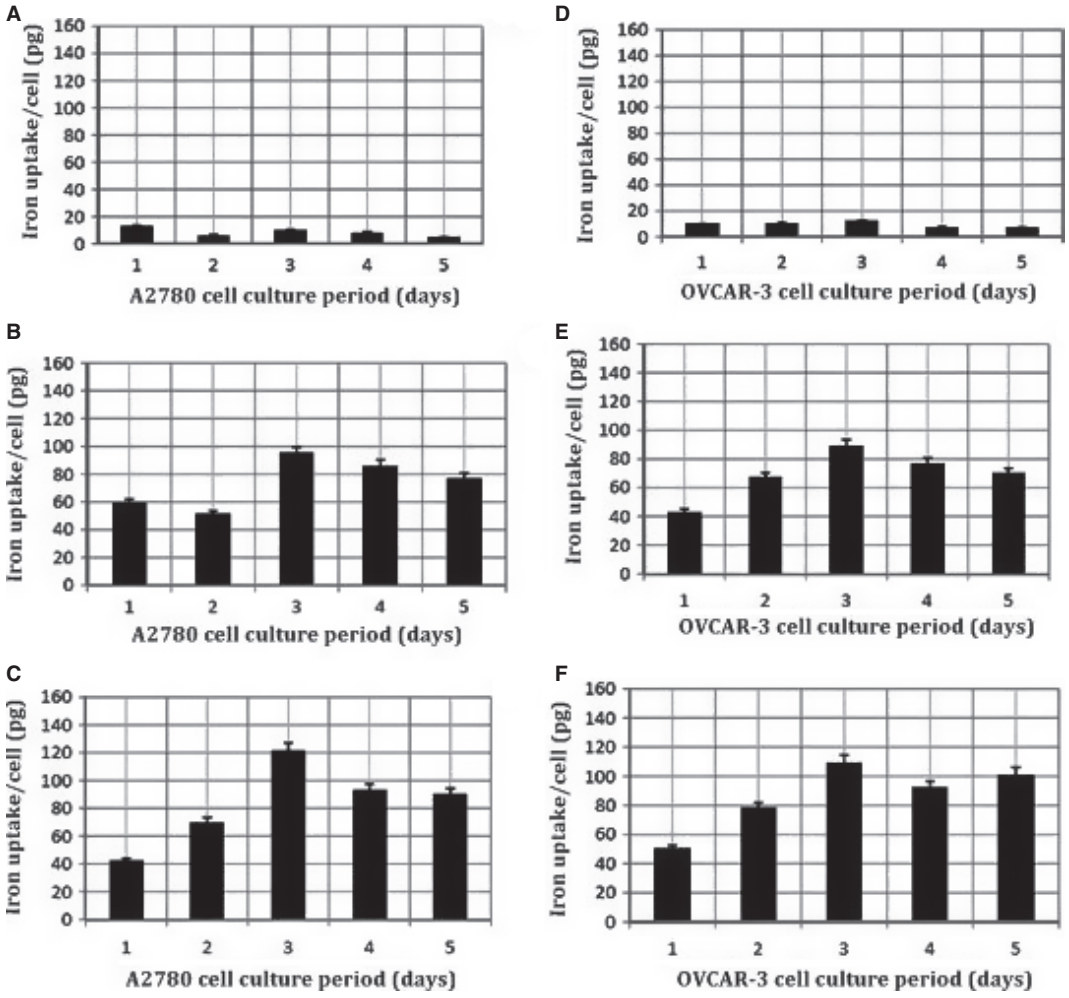

Figure 6: The iron uptake capacity (pg/cell) of A2780 and OVCAR-3 cells when administered with (A, D) bare, (B, E) doxorubicin (DOX) loaded, and (C, F) DOX-loaded chitosan-coated SPIO-NPs for a period of 5 days (120 h), respectively.

(28,29). Previous *in vitro* studies have shown that the inhibition of survivin restores or enhances the chemoreagent cytotoxicity (30). Our results have shown a marked decrease in the expression of bcl-2 and survivin in both of the A2780 and OVCAR-3 human ovarian cancer cell lines after the administration of DOX- chitosan- SPIO-NPs (Figure 7A, B). While, the bax (pro-apoptotic factor) protein was up-regulated during the present experiment. The over-expression of

Table 2: Complete inhibition of A2780 and OVCAR-3 cell-growth after the administration DOX alone, DOX-loaded SPIO-NPs and DOX-loaded chitosan-coated SPIO-NPs for 120 h (5 days)

		Growth inhibition (%)			
Incubation time period (h)	Type of cell line	Control	DOX (0.5 mg/mL)[a]	DOX-loaded chitosan-coated SPIO-NPs	DOX-loaded SPIO-NPs
24	A2780	–	51	74	67
48		–	67	79	71
72		–	74	91	77
96		–	79	98	83
120		–	80	97	86
24	OVCAR-3	–	60	66	64
48		–	67	81	72
72		–	79	90	81
96		–	82	95	84
120		–	80	91	83

DOX, doxorubicin. A2780 and OVCAR-3 cells (5×10^3 cells) were exposed to DOX alone, chitosan-SPIO-NPs, and DOX-loaded chitosan-SPIO-NPs under various time periods (7, 12, 24, 48, and 72 h). The cells were pretreated, separately, for 30 min with DOX alone and DOX-loaded SPIO-NPs. Thus, the cells were pre-incubated for a total of 60 min with DOX and DOX-loaded SPIO-NPs. The final incubation was carried out for above stated time periods in a drug-free medium. These experiments were performed in triplicate. The final cell number was 0.5–1.0 $\times$ 10^5 cells per culture in untreated cultures (100%).
[a]The 0.5 mg/mL DOX was used in all the experiments of DOX alone and chitosan-DOX-SPIO-NPs.

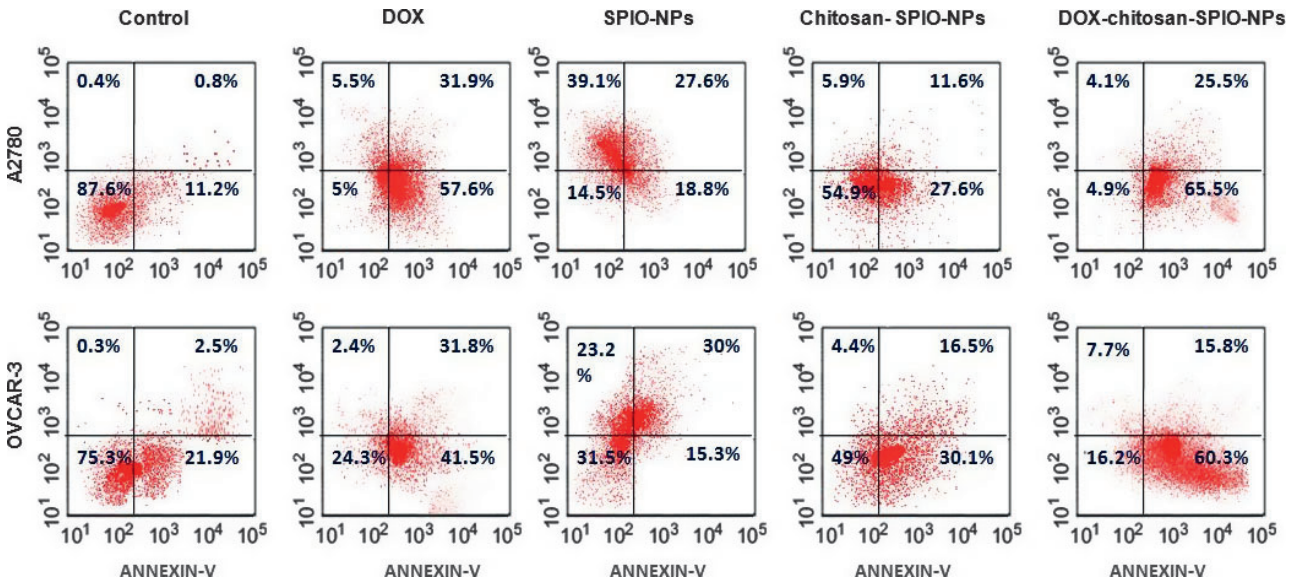

Figure 7: Doxorubicin (DOX)-loaded chitosan-modified SPIO-NP system induces apoptosis in A2780 and OVCAR-3 cells. Both cancer cell lines were treated separately with DOX, SPIO-NPs, chitosan-SPIO-NPs, and DOX-chitosan-SPIO-NPs for 24 h. Apoptotic cell death was detected by staining the cells with Annexin-V-FLUOS kit and analyzed by flow cytometry.

bax has been shown to accelerate cell death (31), while the over-expression of bcl-2 represses the function of bax. So, the ratio of bcl-2/bax can be a critical factor for estimating the cell's capacity for undergoing apoptosis (32). Although, bcl-2 and survivin are both apoptosis inhibitors, they work through different pathways in the apoptotic regulation, which are called the mitochondrial and cytoplasmic pathways, respectively (33). These results have made it clear that the modified nanoparticulate system of drug delivery makes it possible to attack through the intrinsic pathway of cancer cells.

Apoptosis and tumorigenesis are regulated by NF-κB-regulated gene products. The transcription factor NF-κB involves the extrinsic death receptor signaling pathway of apoptosis. Suppression of NF-κB promotes tumor necrosis factor-induced apoptosis (34–36). During the present study, DOX-chitosan-SPIO-NPs decreased the expression of NF-κB in both cell lines. We can assume that the inhibited expression of NF-κB is related to the bcl-2 pathway. The nanoparticulate drug delivery system affects both the intrinsic (mitochondrial) and extrinsic (cytoplasmic) pathways by changing the expression of their regulatory factors

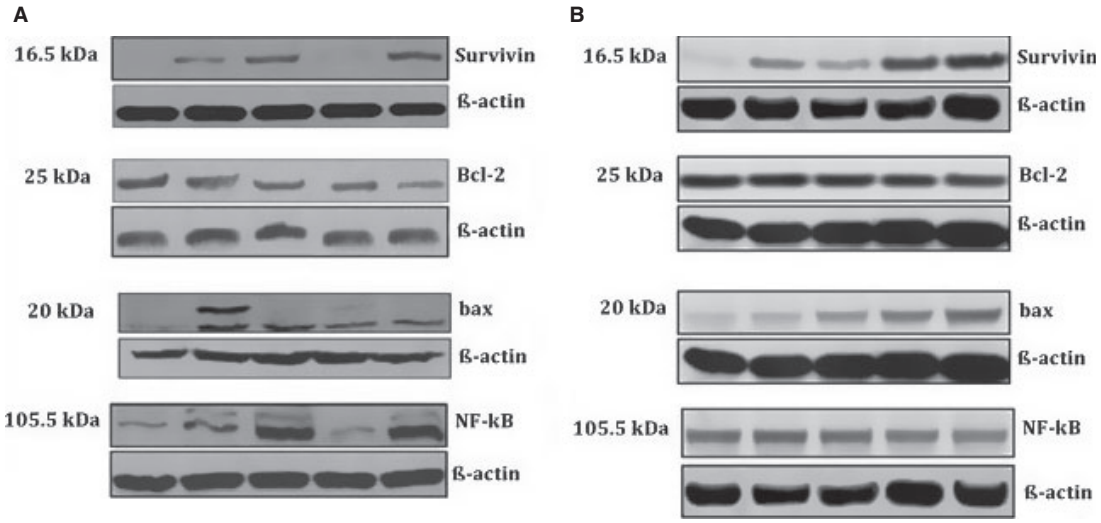

Figure 8: Expression of survivin, bax, bcl-2, and NF-κB proteins in (A) A2780 cells and (B) OVCAR-3 cells by Western blot after 48 h' treatment with bare SPIO-NPs (Column 2), doxorubicin (DOX; Column 3), chitosan-coated SPIO-NPs (Column 4), and DOX-loaded chitosan-coated SPIO-NPs (Column 5). The column 1 shows control experiment.

such as bax and bcl-2, and the transcription factor NF-κB (36).

So, we have demonstrated that biodegradable drug delivery through the nanoparticulate systems can promote apoptosis and lessen the negative effects of chemotherapeutic agents during the *in vitro* conditions. To optimize this drug delivery system, greater understanding of the different mechanisms of biological interactions, and particle engineering, is still required. Further advances are needed in order to turn the concept of nanoparticle technology into a realistic practical application as the next generation of drug delivery system.

References

1. Ferrari M. (2005) Cancer nanotechnology: opportunities and challenges. Nat Rev Cancer;5:161–171.
2. Chertok B., Moffat B.A., David A.E., Yu F., Bergemann C., Ross B.D. (2008) Iron oxide nanoparticles as a drug delivery vehicle for MRI monitored magnetic targeting of brain tumors. Biomaterials;29:487–496.
3. Kikumori T., Kobayashi T., Sawaki M., Imai T. (2009) Anti-cancer effect of hyperthermia on breast cancer by magnetite nanoparticle-loaded anti-HER2 immunoliposomes. Breast Cancer Res Treat;113:435–441.
4. Marchal F., Pic E., Pons T., Dubertret B., Bolotine L., Guillemin F. (2008) Quantum dots in oncological surgery: the future for surgical margin status? Bull Cancer;95:1149–1153.
5. Kim E.H., Lee H.S., Kwak B.K., Kim B.K. (2005) Synthesis of ferrofluid with magnetic nanoparticles by sonochemical method for MRI contrast agent. J Magn Magn Mater;289:328–330.
6. Hong S.W., Chang Y., Hwang M.J., Rhee I., Kang D.S. (2004) Ni-Fe_2O_4 nanoparticles as contrast agents for magnetic resonance imaging. J Korean Soc Magn Reson Med;4:27–32.
7. Ren J., Jia M., Ren T., Yuan W., Tan Q. (2008) Preparation and characterization of PNIPAAm-*b*-PLA/Fe_3O_4 thermo-responsive and magnetic composite micelles. Mater Lett;62:4425–4427.
8. Chandra S., Mehta S., Nigam S., Bahadur D. (2010) Dendritic magnetite nanocarriers for drug delivery applications. New J Chem;34:648–655.
9. Khosroshahi M.E., Ghazanfari L. (2010) Preparation and characterization of silica-coated iron-oxide bionanoparticles under N_2 gas. Physica E;42:1824–1829.
10. Sahoo Y., Pizem H., Fried T., Golodnitsky D., Burstein L., Sukenik S.N., Markovich G. (2001) Alkyl phosphonate/phosphate coating on magnetite nanoparticles: a comparison with fatty acids. Langmuir;17:7907–7911.
11. Nayak S., Lee S., Chmielewski J., Lyon L.A. (2004) Folate-mediated cell targeting and cytotoxicity using thermoresponsive microgels. J Am Chem Soc;126:10258–10259.
12. Mammen M., Choi S.K., Whitesides G.M. (1998) Polyvalent interactions in biological systems: implications for design and use of multivalent ligands and inhibitors. Angew Chem Int Ed;37:2754–2794.
13. Fonseca C., Simões S., Gaspar R. (2002) Paclitaxel-loaded PLGA nanoparticles: preparation, physicochemical characterization and in vitro anti-tumoral activity. J Control Release;83:273–286.
14. Müller B., Kreuter J. (1999) Enhanced transport of nanoparticle associated drugs through natural and artificial membranes – a general phenomenon? Int J Pharm;178:23–32.

15. Xu Y., Du Y. (2003) Effect of molecular structure of chitosan on protein delivery properties of chitosan nanoparticles. Int J Pharm;250:215–226.
16. Qi L.F., Xu Z.R., Jiang X. (2004) Preparation and antibacterial activity of chitosan nanoparticles. Carbohydr Res;339:2693–2700.
17. Artursson P., Lindmark T., Davis S.S., Illum L. (2004) Effect of chitosan on the permeability of monolayers of intestinal epithelial cells (Caco-2). Pharm Res;11:1358–1361.
18. Fernández-Urrusuno R., Calvo P., Remuñán-López C., Vila-Jato J.L., Alonso M.J. (1999) Enhancement of nasal absorption of insulin using chitosan nanoparticles. Pharm Res;16:1576–1581.
19. Vårum K.M., Myhr M.M., Hjerde R.J., Smidsrød O. (1997) In vitro degradation rates of partially *N*-acetylated chitosans in human serum. Carbohydr Res;299:99–101.
20. Miao Y., Tan S.N. (2000) Amperometric hydrogen peroxide biosensor based on immobilization of peroxidase in chitosan matrix crosslinked with glutaraldehyde. Analyst;125:1591–1594.
21. Hong S., Chang Y., Rhee I. (2010) Chitosan-coated ferrite (Fe_3O_4) nanoparticles as a T_2 contrast agent for magnetic resonance imaging. J Korean Phys Soc;56:868–873.
22. Mohammadi-Samani S., Miri R., Salmanpour M., Khalighian N., Sotoudeh S., Erfani S.N. (2013) Preparation and assessment of chitosan-coated superparamagnetic Fe_3O_4 nanoparticles for controlled delivery of methotrexate. Res Pharm Sci;8:25–33.
23. Jain T.K., Morales M.A., Sahoo S.K., Leslie-Pelecky D.L., Labhasetwar V. (2005) Iron oxide nanoparticles for sustained delivery of anticancer agents. Mol Pharm;2:194–205.
24. Gupta A.K., Gupta M. (2005) Synthesis and surface engineering of iron oxide nanoparticles for biomedical applications. Biomaterials;26:3995–4021.
25. Saifuddin N., Dinara S. (2012) Immobilization of *Saccharomyces cerevisiae* onto cross-linked chitosan coated with magnetic nanoparticles for adsorption of Uranium (VI) ions. Adv Nat Appl Sci;6:249–267.
26. Schwertmann U., Cornell R.M. (2007) Iron Oxides in the Laboratory: Preparation and Characterization, 2nd edn. Germany: Wiley-VCH Verlag GmbH; p. 5–18.
27. Hong S., Lim W.T., Rhee I. (2006) Relaxation rate of hydrogen protons of water molecules in an aqueous solution of dextran coated ferrite nanoparticles. J Korean Phys Soc;49:676–681.
28. Chen Y., Mohanraj V.J., Parkin J.E. (2003) Chitosan-dextran sulfate nanoparticles for delivery of an antiangiogenesis peptide. Lett Pept Sci;10:621–627.
29. Vila A., Sanchez A., Tobio M., Calvo P., Alonso M.J. (2002) Design of biodegradable particles for protein delivery. J Control Release;78:15–24.
30. Redhead H.M., Davis S.S., Illum L. (2001) Drug delivery in poly(lactide-co-glycolide) nanoparticles surface modified with poloxamer 407 and poloxamine 908: in vitro characterization and in vivo evaluation. J Control Release;70:353–363.
31. Wang T.T., Wei J., Qian X.P., Ding Y.T., Yu L.X., Liu B.R. (2008) Gambogic acid, a potent inhibitor of survivin, reverses docetaxel resistance in gastric cancer cells. Cancer Lett;262:214–222.
32. Wang L., Zhang G.M., Feng Z.H. (2003) Down-regulation of survivin expression reversed multidrug resistance in adriamycin- resistant HL-60/ADR cell line. Acta Pharmacol Sin;24:1235–1240.
33. Ling X., Bernacki R.J., Brattain M.G., Li F.Z. (2004) Induction of survivin expression by taxol (paclitaxel) is an early event, which is independent of taxol mediated G2/M arrest. J Biol Chem;279:15196–15203.
34. Adams J.M., Cory S. (1998) The Bcl-2 protein family: arbiters of cell survival. Science;281:1322–1326.
35. Kirkin V., Joos S., Zornig M. (2004) The role of Bcl-2 family members in tumorigenesis. Biochim Biophys Acta;1644:229–249.
36. Pandey M.K., Sung B., Ahn K.S. (2007) Gambogic acid, a novel ligand for transferrin receptor, potentiates TNF-induced apoptosis through modulation of the nuclear factor-κB signaling pathway. Blood;110:3517–3525.